

## Superhydrophobic Surfaces of Electrodeposited Polypyrroles Bearing Fluorinated Liquid Crystalline Segments

Thierry Darmanin, Elisabeth Taffin de Givenchy, and Frederic Guittard\*

Université de Nice - Sophia Antipolis, Laboratoire de Chimie des Matériaux Organiques et Métalliques, Equipe Chimie Organique aux Interfaces, Parc Valrose, 06108 Nice Cedex 2, France

Received August 19, 2010; Revised Manuscript Received October 10, 2010

**ABSTRACT:** Two intrinsic properties of fluorinated tails (*F*-butyl to *F*-octyl) were combined in the elaboration of superhydrophobic surfaces by electrochemical polymerization: their promesogenic characteristic and their ability to increase both hydrophobicity and oleophobicity. We report the synthesis and the characterization of pyrrole monomers bearing fluorinated liquid crystalline segments. The electrodeposited corresponding polymer films were characterized by cyclic voltammetry, static and dynamic contact angle measurements, and scanning electron microscopy. Sticky superhydrophobic surfaces were obtained with a *F*-hexyl or a *F*-octyl tail. The presence of mesogenic segments improves the surface hydrophobicity and increases the surface roughness, clearly observed with *F*-butyl and *F*-hexyl chains.

### Introduction

Highly fluorinated tails have exceptional intrinsic properties allowing their use in a large domain of applications going from hydrophobic materials to liquid-crystalline compounds.<sup>1,2</sup> Thus, their introduction in an amphiphilic structure could lead to the formation of well-organized mesophases. Their introduction in a polymer decreases its surface energy due to the orientation of the fluorinated tail at the extreme surface. However, the contact angle with water on flat surface is rarely above 120° whatever the length of the fluorinated tail or their proportion.<sup>3–5</sup> Moreover, in a polar environment, the fluorinated tails at the extreme surface undergo rearrangements limiting their use. Takahara et al.<sup>6</sup> showed that the surface rearrangements are depending on the length of the fluorinated tail. For long fluorinated tails (more than eight fluoromethylene units), strong interactions are present between the fluorinated tail leading to their crystallization and reducing their mobility. For short fluorinated tails (less than 6 fluoromethylene units), no crystallization was observed and the dynamic surface properties were poor. Recently, to counter the problem, the concept of mesogenic core, inserted between the fluorinated tail and the polymer chain, was reported.<sup>7</sup> These mesogenic cores decreased the mobility of the fluorinated tails and thus improved the antiwetting properties.

Fluorinated tails can also be used for the elaboration of superhydrophobic surfaces, which have recently attracted much interest because of their potential applications in many fields.<sup>8–12</sup> In this domain, according to the Wenzel and Cassie–Baxter theories,<sup>13–15</sup> the contribution of physical parameters (roughness and morphology) in addition to chemical parameters (fluorinated tail for example) allowed to enhance the surface antiwetting properties. Among the reported methods, the electrochemical polymerization of hydrophobic monomers<sup>16–21</sup> is a choice method (one-pot, mild conditions, morphology adjustable) for the elaboration of micro- or nanostructured surfaces. Thus, it has been demonstrated that the electrochemical polymerization of semifluorinated thiophenes,<sup>18</sup> pyrroles,<sup>19,20a</sup> 3,4-ethylenedioxythiophenes,<sup>18,20</sup> and 3,4-alkylenedioxythiopyrroles<sup>18,21</sup> allowed the deposition of films with excellent antiwetting properties.

Here, in order to combine the effect of mesogenic core in the electrochemical polymerization of fluorinated monomers, a phenyl ring was inserted between the semifluorinated tail and the electropolymerizable pyrrole moiety. A schematic representation of the studied monomers is given in Scheme 1a. We report the synthesis of the monomers, their electrochemical polymerization, and the evaluation of the surface properties of the corresponding conductive polymers by static and dynamic contact angles, imaging infrared, optical profilometry, and scanning electron microscopy. Their surface properties will be compared to the previously reported fluorinated polypyrroles represented in Scheme 1b.

### Experimental Section

**Materials.** All chemical products were purchased from Sigma-Aldrich. Electrochemical grade of tetrabutylammonium hexafluorophosphate was chosen. Gold plates (deposition of Cr + Au 1500 Å on silicon wafers) were purchased from Neyco.

**Measurements.** The mass spectra were obtained by electron ionization at 70 eV with a Thermo TRACEGC of Thermo-fischer Corp. fitted with an Automass III Multi spectrometer. The retention times of the compounds were determined with a 5890 series II gas chromatography from Hewlett-Packard equipped with a capillary column HP5 (30 m, 0.32 mm): the heating program is 60–250 °C at 10 °C/min and 30 min at 250 °C, and the standard reference is heptane. NMR spectra were realized with a Bruker W-200 MHz. The melting points and the thermal analyses were obtained with a Jade DSC of Perkin-Elmer with scan rates of 10 °C/min. The polarized optical microscopy (POM) images were obtained with an Olympus BX60. Electrochemical experiments were performed with an Autolab PGSTAT 30 potentiostat from Eco Chemie B.V. equipped with General Purpose Electrochemical System (GPES) software and connected to a three-electrode cell. A platinum disk (area = 7.1 mm<sup>2</sup>) or a gold plate (area = a few cm<sup>2</sup>) was used as working electrode, a glassy carbon rod as counter electrode, and a saturated calomel electrode (SCE) as reference electrode. Static and dynamic contact angle measurements (average of five measurements) were performed with a Krüss DSA-10 contact angle goniometer at 21 ± 1 °C. The sliding angle and the hysteresis were determined by the tilted-drop method with 6 μL water

\*Corresponding author. E-mail: Frederic.GUITTARD@unice.fr.

droplets. Infrared surface images were obtained in reflection with a Spotlight 3100 FTIR microscope from Perkin-Elmer equipped with a Spectrometer 100. Roughness parameters were obtained with a WYKO NT1100 optical profiling system from Veeco. Scanning electron microscopy (SEM) images were obtained with a JEOL 6700F microscope.

**Synthesis of Molecules 1, 2, and 3.** The synthesis of compounds **2** and **3**, represented in Scheme 2, was previously reported.<sup>22–24</sup> Compound **1** was synthesized by a similar route.

**1:** *S*-3,3,4,4,5,5,6,6,6-Nonafluorohexyl-4-hydroxybenzothioate.  $\delta_{\text{H}}$  (200 MHz, MeOD): 7.77 (d,  $^3J_{\text{HH}} = 8.8$  Hz, 2H), 6.78 (d,  $^3J_{\text{HH}} = 8.8$  Hz, 2H), 3.18 (t,  $^3J_{\text{HH}} = 7.8$  Hz, 2H), 2.49 (tt,  $^3J_{\text{HH}} = 7.8$ ,  $^3J_{\text{HF}} = 17.8$ , 2H).  $\delta_{\text{F}}$  (188 MHz, MeOD): -81.08 (m, 3F), -116.14 (m, 2F), -125.91 (m, 2F), -127.66 (m, 2F).

**Synthesis of the Monomers 4, 5, and 6.** 2-(1*H*-pyrrol-3-yl)acetic acid was synthesized by a procedure developed by Lemaire et al.<sup>25–27</sup> *N*-(3-(Dimethylamino)propyl)-*N'*-ethylcarbodiimide hydrochloride (EDC) (1.0 g, 5.2 mmol) was added to a solution of 2-(1*H*-pyrrol-3-yl)acetic acid (0.65 g, 5.2 mmol) in acetonitrile. After stirring for 30 min at room temperature, 2-*F*-alkylethyl-4-hydroxythiobenzoate (**1–3**) (5.2 mmol) was added. After a day, the solvent was removed and the crude was purified by column chromatography (silica gel; eluent: dichloromethane) to yield the products as white solids.

**4:** 4-((3,3,4,4,5,5,6,6,6-Nonafluorohexylthio)carbonyl)phenyl 2-(1*H*-Pyrrol-3-yl)acetate. Yield 45%; tr = 22.9 min.  $\delta_{\text{H}}$  (200 MHz, CDCl<sub>3</sub>): 8.22 (s, 1H), 7.97 (d,  $^3J_{\text{HH}} = 8.8$  Hz, 2H), 7.21 (d,  $^3J_{\text{HH}} = 8.8$  Hz, 2H), 6.81 (m, 2H), 6.27 (dd,  $^3J_{\text{HH}} = 4.2$  Hz,  $^4J_{\text{HH}} = 2.5$  Hz, 1H), 3.79 (s, 2H), 3.28 (t,  $^3J_{\text{HH}} = 7.8$  Hz, 2H), 2.49 (tt,  $^3J_{\text{HH}} = 7.8$  Hz,  $^3J_{\text{HF}} = 17.8$  Hz, 2H).  $\delta_{\text{C}}$  (50 MHz, CDCl<sub>3</sub>): 189.67, 170.17, 155.19, 133.81, 128.77, 121.97, 118.33, 116.78, 114.51, 109.21, 33.12, 31.63 (t,  $^2J_{\text{CF}} = 21.9$  Hz), 20.12 (t,  $^3J_{\text{CF}} = 4.6$  Hz).  $\delta_{\text{F}}$  (188 MHz, CDCl<sub>3</sub>): -81.42 (m, 3F), -115.17 (m, 2F), -124.77 (m, 2F), -126.45 (m, 2F). FTIR (main vibrations):  $\nu = 3406$  (N–H), 2921, 2855, 1749 (OC=O), 1660 (SC=O), 1599, 1500, 1242, 1215, 1130 cm<sup>-1</sup>. MS (70 eV): *m/z* (%): 507 (1) [M<sup>+</sup>], 228 (7) [C<sub>13</sub>H<sub>10</sub>O<sub>3</sub>N<sup>+</sup>], 121 (47) [C<sub>7</sub>H<sub>4</sub>O<sub>2</sub><sup>+</sup>], 80 (100) [C<sub>5</sub>H<sub>6</sub>N<sup>+</sup>].

**5:** 4-((3,3,4,4,5,5,6,6,7,7,8,8,8-Tridecafluorooctylthio)carbonyl)phenyl 2-(1*H*-Pyrrol-3-yl)acetate. Yield 32%; tr = 24.5 min.  $\delta_{\text{H}}$  (200 MHz, CDCl<sub>3</sub>): 8.22 (s, 1H), 7.97 (d,  $^3J_{\text{HH}} = 8.8$  Hz, 2H), 7.21 (d,  $^3J_{\text{HH}} = 8.8$  Hz, 2H), 6.81 (m, 2H), 6.27 (dd,  $^3J_{\text{HH}} = 4.2$  Hz,  $^4J_{\text{HH}} = 2.5$  Hz, 1H), 3.79 (s, 2H), 3.28 (t,  $^3J_{\text{HH}} = 7.8$  Hz, 2H), 2.49 (tt,  $^3J_{\text{HH}} = 7.8$  Hz,  $^3J_{\text{HF}} = 17.8$  Hz, 2H).  $\delta_{\text{C}}$  (50 MHz,

CDCl<sub>3</sub>): 189.67, 170.18, 155.19, 133.81, 128.77, 121.97, 118.33, 116.78, 114.51, 109.21, 33.12, 31.73 (t,  $^2J_{\text{CF}} = 21.9$  Hz), 20.15 (t,  $^3J_{\text{CF}} = 4.6$  Hz).  $\delta_{\text{F}}$  (188 MHz, CDCl<sub>3</sub>): -81.20 (m, 3F), -114.93 (m, 2F), -122.31 (m, 2F), -123.28 (m, 2F), -123.80 (m, 2F), -126.56 (m, 2F). FTIR (main vibrations):  $\nu = 3406$  (N–H), 2921, 2853, 1748 (OC=O), 1663 (SC=O), 1595, 1500, 1242, 1211, 1143 cm<sup>-1</sup>. MS (70 eV): *m/z* (%): 607 (2) [M<sup>+</sup>], 228 (9) [C<sub>13</sub>H<sub>10</sub>O<sub>3</sub>N<sup>+</sup>], 121 (40) [C<sub>7</sub>H<sub>4</sub>O<sub>2</sub><sup>+</sup>], 80 (100) [C<sub>5</sub>H<sub>6</sub>N<sup>+</sup>].

**6:** 4-((3,3,4,4,5,5,6,6,7,7,8,8,9,9,10,10,10-Heptafluorodecylthio)carbonyl)phenyl 2-(1*H*-Pyrrol-3-yl)acetate. Yield 25%; tr = 26.4 min.  $\delta_{\text{H}}$  (200 MHz, CDCl<sub>3</sub>): 8.22 (s, 1H), 7.97 (d,  $^3J_{\text{HH}} = 8.8$  Hz, 2H), 7.21 (d,  $^3J_{\text{HH}} = 8.8$  Hz, 2H), 6.81 (m, 2H), 6.27 (dd,  $^3J_{\text{HH}} = 4.2$  Hz,  $^4J_{\text{HH}} = 2.5$  Hz, 1H), 3.79 (s, 2H), 3.28 (t,  $^3J_{\text{HH}} = 7.8$  Hz, 2H), 2.49 (tt,  $^3J_{\text{HH}} = 7.8$  Hz,  $^3J_{\text{HF}} = 17.8$  Hz, 2H).  $\delta_{\text{C}}$  (50 MHz, CDCl<sub>3</sub>): 189.67, 170.17, 155.19, 133.82, 128.78, 121.97, 118.33, 116.78, 114.52, 109.22, 33.13, 31.75 (t,  $^2J_{\text{CF}} = 21.9$  Hz), 20.15 (t,  $^3J_{\text{CF}} = 4.6$  Hz).  $\delta_{\text{F}}$  (188 MHz, CDCl<sub>3</sub>): -81.17 (m, 3F), -114.88 (m, 2F), -122.28 (m, 6F), -123.13 (m, 2F), -123.76 (m, 2F), -126.52 (m, 2F). FTIR (main vibrations):  $\nu = 3406$  (N–H), 2921, 2853, 1748 (OC=O), 1663 (SC=O), 1595, 1500, 1242, 1215, 1147 cm<sup>-1</sup>. MS (70 eV): *m/z* (%): 707 (2) [M<sup>+</sup>], 228 (13) [C<sub>13</sub>H<sub>10</sub>O<sub>3</sub>N<sup>+</sup>], 121 (37) [C<sub>7</sub>H<sub>4</sub>O<sub>2</sub><sup>+</sup>], 80 (100) [C<sub>5</sub>H<sub>6</sub>N<sup>+</sup>].

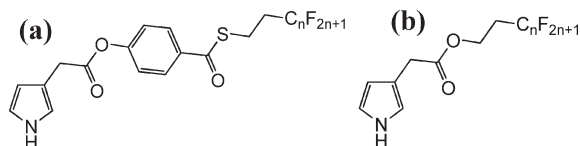
## Results and Discussion

**Monomer Synthesis.** Pyrrole unit was chosen because of its high polymerization ability. Indeed, as the liquid crystal (LC) segments are very bulky, the replacement of the pyrrole unit by a thiophene one, which has a lower polymerization ability, gave nonpolymerizable monomers. Scheme 2 shows the LC segments used in this work; they consisted in a promesogenic semifluorinated tail bound to a phenyl by a thioester connector. These LC units were already been incorporated for the synthesis of other LC molecules.<sup>22–24</sup> Their introduction, for example, inside a polyacrylate backbone allowed to amplify and stabilize the surface antiwetting properties by structuring the orientation of the fluorinated chains.<sup>24</sup> The use of a thioester connector is very important for the liquid-crystalline properties.<sup>22</sup>

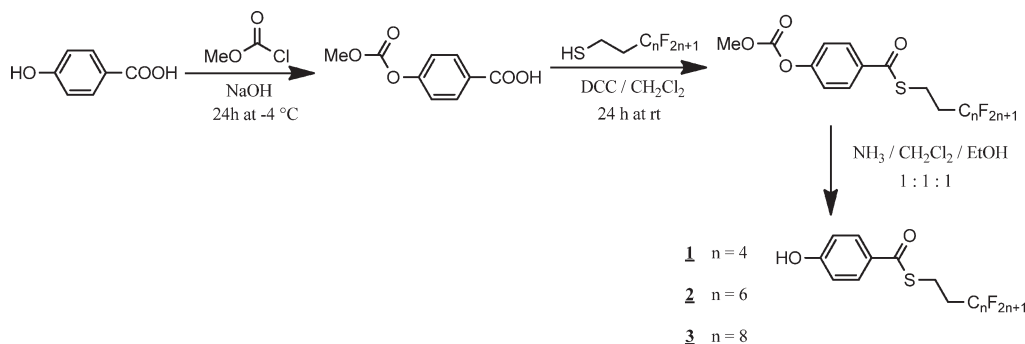
2-*F*-Alkylethyl-4-hydroxythiobenzoates were obtained from 4-hydroxybenzoic acid in excellent global yields and in three steps from 4-hydroxybenzoic acid (Scheme 2): hydroxyl group protection using methyl chloroformate, coupling of semifluorinated thiol, and hydroxyl group deprotection with a mixture of ammonium hydroxide (28% in water), dichloromethane, and ethanol (1:1:1).

Then, 2-(1*H*-pyrrol-3-yl)acetic acid was synthesized from pyrrole in four steps and following the general pathway described by Lemaire et al.<sup>25–27</sup> This synthetic route includes the nitrogen protection with tosyl chloride, the acylation at the 3-position of pyrrole by Friedel–Crafts acylation using aluminum chloride and acetic anhydride, the transposition

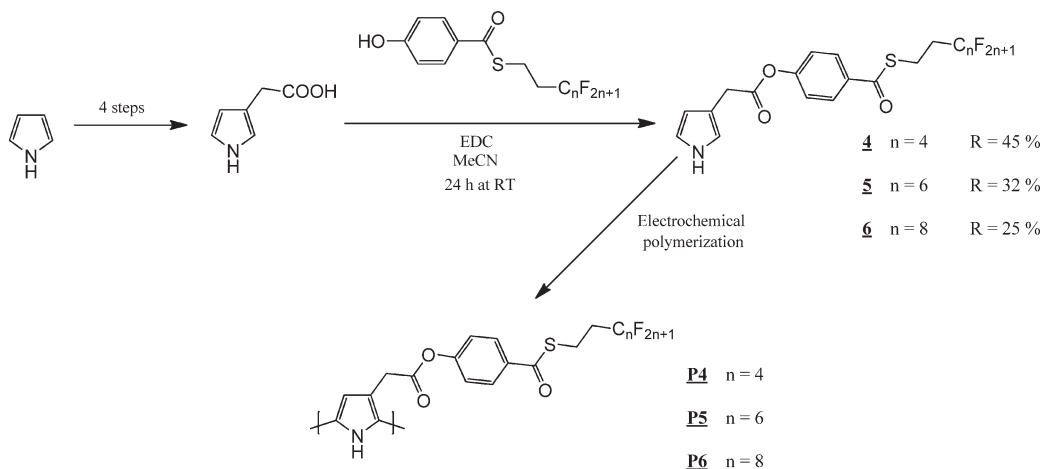
**Scheme 1.** (a) Studied Monomers and (b) Previously Reported<sup>19</sup> Pyrrole Derivatives ( $n = 4, 6, \text{ and } 8$ )



**Scheme 2.** Synthesis of the LC Segments



Scheme 3. Synthesis of the Monomers and Corresponding Polymers



of the acetyl to methyl acetate group by Willgerodt–Kindler reaction using thallium(III) nitrate, trimethyl orthoformate and montmorillonite K10, the hydrolysis of the ester function, and the tosyl group with an aqueous solution of sodium hydroxide.

Finally, fluorinated LC segments were grafted to a pyrrole moiety to give monomers **4–6** as described in Scheme 3. These monomers were synthesized by coupling the LC segments with 2-(1*H*-pyrrol-3-yl)acetic acid. The synthesis was performed in acetonitrile with *N*-(3-(dimethylamino)propyl)-*N'*-ethylcarbodiimide hydrochloride (EDC) as coupling agents. The monomers were obtained in 25–45% isolated yields. The insertion of the semifluorinated LC segment was confirmed by  $^1\text{H}$  NMR,  $^{13}\text{C}$  NMR,  $^{19}\text{F}$  NMR, FTIR (large ester band at  $1748\text{ cm}^{-1}$  and thioester at  $1663\text{ cm}^{-1}$ ), and mass spectrometry (presence of the molecular ion).

**Liquid Crystalline Behavior of the Monomers.** The liquid crystalline behavior of the monomers was determined by combining thermal analyses obtained by differential scanning calorimetry (DSC) and optical images obtained by polarizing optical microscopy (POM). The thermal analyses by DSC, at a scanning rate of  $10\text{ °C min}^{-1}$  (cf. Supporting Information), showed an enantiotropic mesomorphic behavior of the monomers **5** and **6**, which contain a perfluorohexyl (*F*-hexyl) or a perfluorooctyl tail (*F*-octyl), respectively. Mesophases were detectable on both heating and cooling. For monomer **4**, which contains a perfluorobutyl (*F*-butyl), the mesophase was observed in a temperature range of less than  $1\text{ °C}$  on cooling, which revealed a monotropic behavior. The solid–liquid crystal and liquid crystal–liquid transition temperatures and temperature ranges of the mesophases increased with the lengthening of the fluorinated tail. During the heating, the temperature range of the mesophases was about  $38\text{ °C}$  for **6** and  $12\text{ °C}$  for **5**. During the cooling, two crystalline phases were observed for **6**. The phase diagram of the compound as a function of the *F*-alkyl length is given in Figure 1. The LC mesophases were confirmed by polarized optical microscopy (POM) (Figure 2). The mesophases appear as batonnets and after coalescence gave rise to fan-shaped textures with focal-conic domains, which are characteristic of smectic mesophases.<sup>28</sup>

**Electropolymerization.** The electrochemical polymerization of the monomers was performed in an anhydrous acetonitrile solution containing  $0.01\text{ M}$  of the monomer and  $0.1\text{ M}$  of tetrabutylammonium hexafluorophosphate ( $\text{Bu}_4\text{NPF}_6$ ). Single scan by voltammetry cyclic gave the

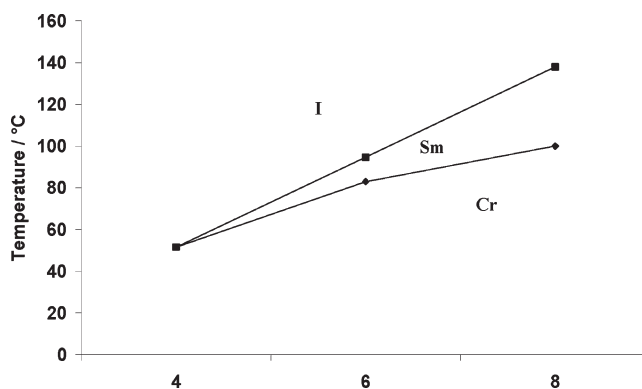


Figure 1. Phase diagram for the monomers **4**, **5**, and **6** with 4, 6, and 8 fluoromethylene units, respectively (I = isotropic, Sm = smectic, Cr = crystalline).



Figure 2. Optical polarizing micrograph of **6** on cooling. Magnification  $\times 33$ ;  $T = 134\text{ °C}$ .

maximum of the oxidation potential peak of the monomers ( $E_{\text{peak,m}}^{\text{ox}}$ ). The value of  $E_{\text{peak,m}}^{\text{ox}}$  is about  $1.28\text{ V}$  vs SCE for the three monomers (Table 1), in comparison of the  $1.25\text{ V}$  for pyrrole. Indeed, the methylene spacer and the ester connector inhibited the electron-withdrawing and electron-donating effects of the substituents. The polymerizability of the monomers was studied by consecutive voltammetric scans from a potential lower to the reduction potential of the polymer and until a potential slightly lower than  $E_{\text{peak,m}}^{\text{ox}}$ .

**Table 1. Electrochemical Data of the Monomers and Their Corresponding Polymers (Potentials in V vs SCE)<sup>a</sup>**

monomer	$E_{\text{peak,m}}^{\text{ox}}$	$E_{\text{p,opt}}^{\text{ox}}$	$E_{\text{polymer}}^{\text{ox}}$	$E_{\text{polymer}}^{\text{red}}$
4	1.28	1.17	0.03/0.38	-0.06/0.28
5	1.29	1.17	0.31/0.69	u/0.51
6	1.29	1.17	0.06/0.95	0.09/0.55
pyrrole	1.25	1.15	0.08	0.07

<sup>a</sup> u = undetermined;  $E_{\text{p,opt}}^{\text{ox}}$  = optimal oxidation potential of the monomer.

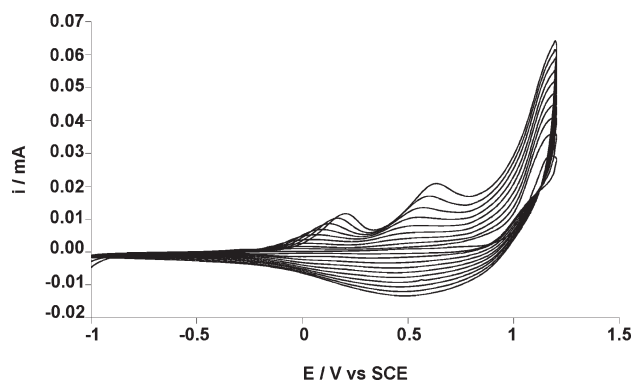


**Figure 3.** Cyclic voltammogram of the monomer **5** (0.01 M) on Pt electrode recorded in 0.1 M  $\text{Bu}_4\text{NPF}_6/\text{CH}_3\text{CN}$ : 10 scans.

**Table 2. Wettability and Roughness Parameters**

	$Q_s$ [ $\text{mC cm}^{-2}$ ]	static contact angles [deg] of water	roughness parameters [nm]	
			$R_a$	$R_q$
<b>P4</b>	150	119	330	512
<b>P5</b>	150	154	372	641
	75	121	86	160
	25	106	14	21
<b>P6</b>	150	153	351	572

denoted  $E_{\text{p,opt}}^{\text{ox}}$ . A continuous growth of polymer film at the electrode surface was observed for all the pyrrole derivatives (Figure 3). The cyclic voltammograms of the three substituted polymers showed two oxidation and reduction peaks, which are an evidence of an electroactive polymer on the surface. The electrochemical data of the polymers are given in Table 1. In order to determine the wettability and the morphology of the surfaces, the polymers were electrochemically deposited on gold plates by chronoamperometry (imposed potential of 1.17 V) with a deposition charge ( $Q_s$ ) of  $150 \text{ mC cm}^{-2}$ . This deposition charge gave the best contact angles (see Table 2 for **P5**).

**Surface Analyses and Discussion.** Figure 4 shows the contact angles (CA) determined with  $2 \mu\text{L}$  water ( $\gamma_L = 72.8 \text{ mN/m}$ ), diiodomethane ( $\gamma_L = 50.0 \text{ mN/m}$ ), and hexadecane ( $\gamma_L = 27.6 \text{ mN/m}$ ) droplets. The contact angle values were similar when *F*-hexyl or *F*-octyl tail was used but a decrease of about  $20^\circ$  with water was observed with *F*-butyl tail. The films **P5** and **P6** exhibited superhydrophobic properties ( $\text{CA}_{\text{water}}$  higher than  $153^\circ$ ) and almost oleophobic properties ( $\text{CA}_{\text{hexadecane}} \approx 74^\circ$ ), whereas nonsubstituted polypyrrole was, in the same condition of preparation, hydrophilic and superoleophilic. In comparison with previously reported fluorinated polypyrroles (Scheme 1b),<sup>19</sup> the presence of the LC segment increased the water contact angle of about  $10^\circ$ – $25^\circ$  following the length of the fluorinated tail. Indeed,  $\text{CA}_{\text{water}} = 136^\circ$ ,  $130^\circ$ , and  $108^\circ$  for the monomers without LC segments represented in Scheme 1b and substituted with a *F*-octyl, *F*-hexyl, and *F*-butyl tail, respectively.

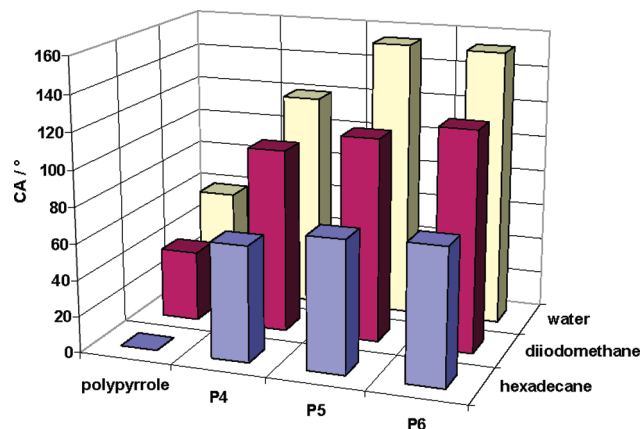


**Figure 4.** Static contact angles of the polymer surfaces ( $Q_s \approx 150 \text{ mC cm}^{-2}$ ).

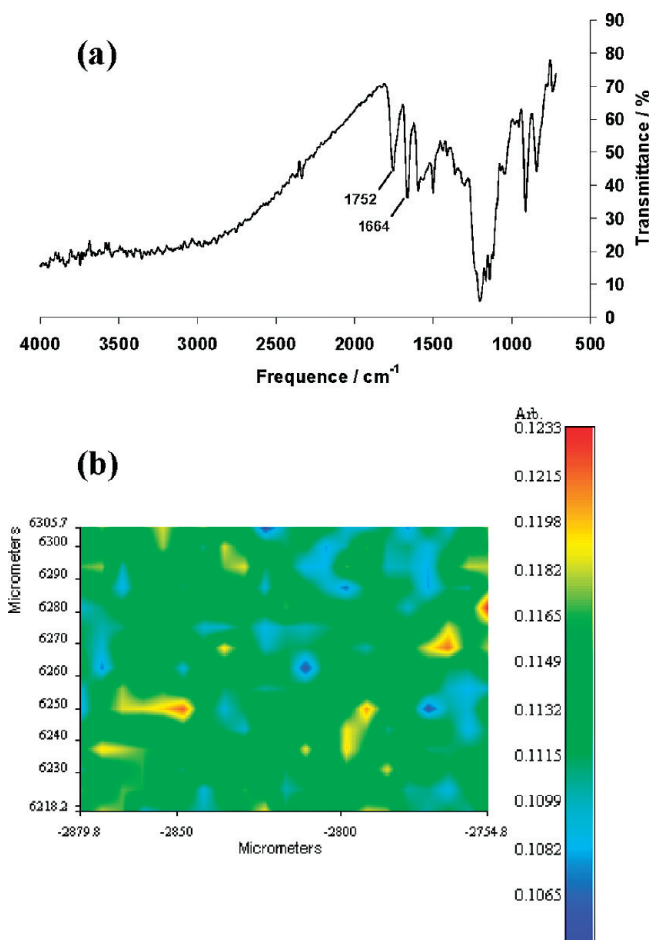


**Figure 5.** (a) Infrared spectra of **P5** obtained by imaging infrared and (b) surface distribution of the ester function.

Moreover, although **P5** and **P6** exhibited a superhydrophobic behavior, the dynamic contact angle measurements by the tilted-drop method revealed water droplets did not roll off the surface when this one was inclined even with a high tilt angle ( $90^\circ$ ), which means that the hysteresis was very high as already observed in previous papers.<sup>18,19,29,30</sup> To confirm this important data, water droplets were deposited on the surfaces, and after penetration of the syringe inside the droplet, the droplet volume was increased and then reduced to determine the advanced and receding contact angles, respectively. Using this method, the advanced and receding

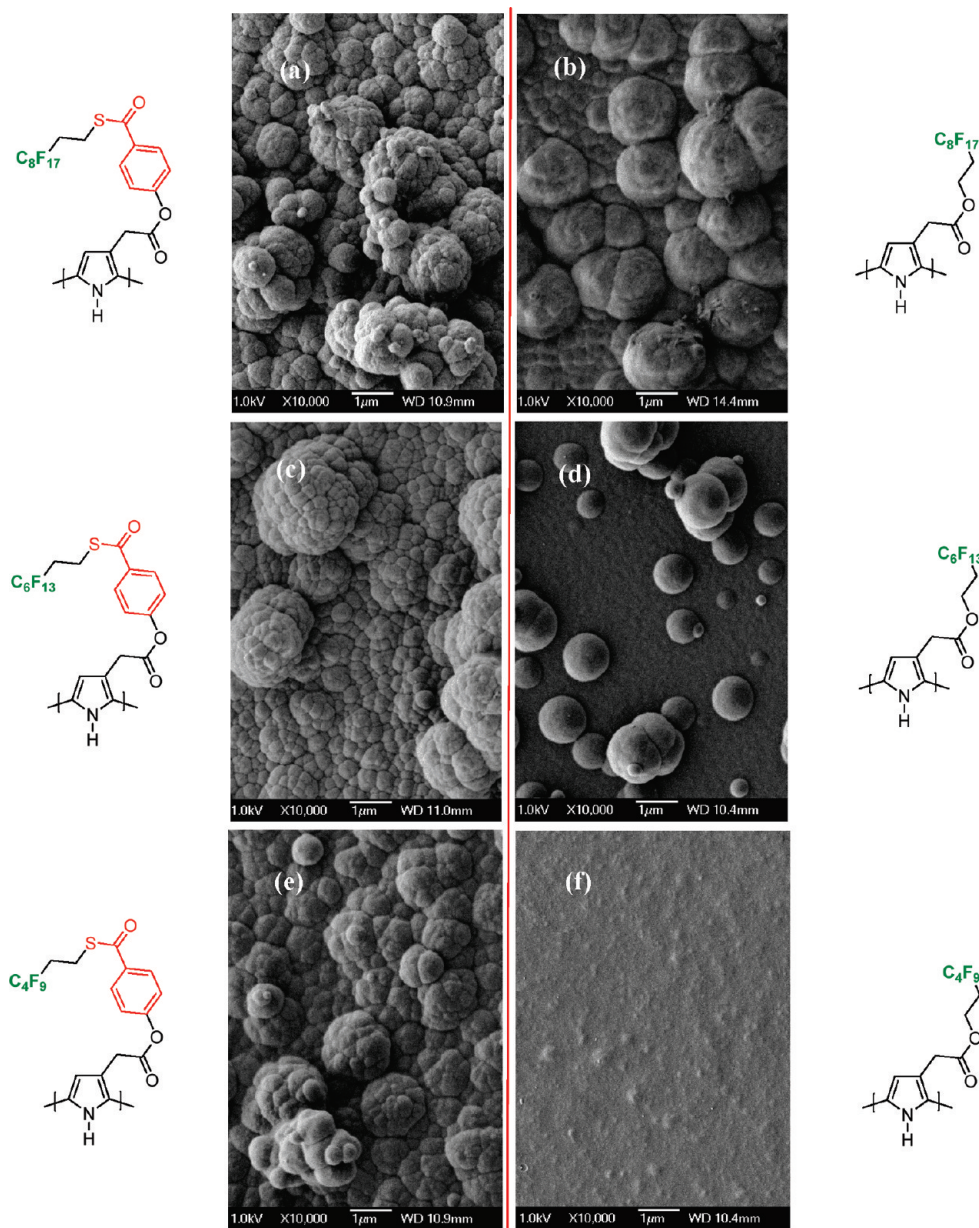


**Figure 6.** SEM images of (a) P6, (c) P5, and (e) P4 and (b, d, f) their homologues without LC segment. The scale bar represents 1  $\mu\text{m}$ . Substrate: gold; salt:  $\text{Bu}_4\text{NPF}_6$ ;  $Q_s \approx 150 \text{ mC cm}^{-2}$ .

contact angles should be determined when the triple point moves. However, if it was possible to determine the advanced contact angle, the triple point did not move during the reduction of the droplet volume, which confirms the very low receding contact angle and as a consequence the very high hysteresis. Surfaces with both high water contact angle and large contact angle hysteresis are known as “highly adhesive surfaces”.<sup>31</sup> These particular surface properties give to the gecko its ability to climb vertical surfaces and was also observed on the petals’ surfaces of red roses.<sup>31</sup>

This result assumes that the increase in roughness increased the water contact angles but also the hysteresis because of the possibility of water to penetrate inside the roughness. Thus, even if the liquid-crystal segments can improve the dynamic contact angles,<sup>7</sup> in this case, this improvement was canceled by the increase of the hysteresis as a function of the surface roughness. To verify this assumption, the surface morphology was investigated by imaging infrared, optical profilometry, and SEM.

The surface were analyzed by imaging infrared in reflection mode (polymer deposition on gold plate). First, these analyses allowed to obtain the infrared spectra of the polymers, as shown in Figure 5a. The polymers were confirmed especially by the presence of two peaks: a large ester band at  $1752 \text{ cm}^{-1}$  and a large thioester band at  $1664 \text{ cm}^{-1}$ . Second, this analysis technique was used to achieve a surface functional distribution by focusing on one chemical function. Here, the focusing on the ester function, as shown in Figure 5b, revealed variations of functional distribution probably due to surface roughness. To confirm this hypothesis and to determine the surface roughness and morphology, the surfaces were analyzed by optical profilometry and SEM.

The study of the surface roughness by optical profilometry (Table 2 and Supporting Information) revealed that the surface roughness of the electrodeposited films was quite similar for the same deposition charge whatever the fluorinated chain length ( $330 \text{ nm} < R_a < 372 \text{ nm}$ ). The heights of the biggest agglomerates were between 3.0 and 4.5  $\mu\text{m}$ .

The Wenzel roughness factors were calculated for P5 from the surface obtained with  $Q_s = 25 \text{ mC/cm}^{-2}$  ( $R_a = 14 \text{ nm}$ ) which was considered as a smooth surface (see Table 2). Thus, the roughness parameters for P5 using the Wenzel model are  $r = \cos(121^\circ)/\cos(106^\circ) = 1.87$  for  $Q_s = 75 \text{ mC cm}^{-2}$  and  $r = \cos(154^\circ)/\cos(106^\circ) = 3.26$  for  $Q_s = 150 \text{ mC cm}^{-2}$ .

Figure 6a,c,e shows SEM images of P4, P5, and P6 surfaces obtained by electrochemical polymerization. The surface morphology consisted in an assembly of micrometric cauliflower-like structures, which are similar to the structures obtained with fluorinated polypyrroles,<sup>19</sup> polythiophenes,<sup>18</sup> or poly(3,4-propylenedioxyppyrrrole).<sup>21</sup> The presence of the LC segment did not modify the nature of the morphology. However, it is clear that the LC segment increases the abundance of the surface microstructures especially observed with *F*-hexyl and *F*-butyl chains (Figure 6c–f), in agreement with their wettability, even if the surface antiwetting properties are the consequence of both the surface roughness–morphology and surface chemistry. For example, in the case of *F*-butyl chains, smooth surfaces<sup>19</sup> were obtained without LC segment (Figure 6f) and micrometric cauliflower microstructures with it (Figure 6e).

## Conclusion

Here, we report the synthesis and characterization of pyrrole derivatives bearing semifluorinated liquid-crystalline segments. These monomers were employed for the elaboration of superhydrophobic polymer films deposited by electrochemical polymerization. Superhydrophobic and oleophobic films with a sticky behavior were obtained using a *F*-hexyl and a *F*-octyl tail. The surface morphology consisted in cauliflower-like microstructures and was independent of the fluorinated tail length. The presence of LC behavior from monotropic ( $F_4$ ) to enantiotropic ( $F_6$ ,  $F_8$ ) seems to be in strong correlation with the modification of wettability. In comparison with previously reported fluorinated pyrroles, the presence of the LC segment improved the surface hydrophobicity by increasing the surface structuration switching hydrophobic to superhydrophobic materials (P5, P6) and opening new way for the development of antiwetting electro-optical devices.

**Supporting Information Available:** DSC curves of the monomers and optical profilometer images of the polymers. This material is available free of charge via the Internet at <http://pubs.acs.org>.

## References and Notes

- Gladysz, J. A.; Curran, D. P.; Horváth, I. T. *Handbook of Fluorous Chemistry*; Wiley-VCH Verlag GmbH & Co. KGaA: Weinheim, 2004.
- Kirsch, P. *Modern Fluoroorganic Chemistry*; Wiley-VCH Verlag GmbH & Co. KGaA: Weinheim, 2004.
- Hayakawa, T.; Wang, J.; Xiang, M.; Li, X.; Ueda, M.; Ober, C. K.; Genzer, J.; Sivaniah, E.; Kramer, E. J.; Fisher, D. A. *Macromolecules* **2000**, *33*, 8012–8019.
- Grundke, K.; Pospiech, D.; Kolling, W.; Simon, F.; Janke, A. *Colloid Polym. Sci.* **2001**, *279*, 727–735.
- Xiang, M.; Li, X.; Ober, C. K.; Char, K.; Genzer, J.; Sivaniah, E.; Kramer, E. J.; Fisher, D. A. *Macromolecules* **2000**, *33*, 6106–6119.
- Honda, K.; Morita, M.; Otsuka, H.; Takahara, A. *Macromolecules* **2005**, *38*, 5699–5705.
- Caillier, L.; Taffin de Givenchy, E.; G ribaldi, S.; Guittard, F. *J. Mater. Chem.* **2008**, *18*, 5382–5389 and references therein.
- Li, X.-M.; Reinhoudt, D.; Crego-Calama, M. *Chem. Soc. Rev.* **2007**, *36*, 1350–1368.
- Zhang, X.; Shi, F.; Niu, J.; Jiang, Y.; Wang, Z. *J. Mater. Chem.* **2008**, *18*, 621–633.
- Ma, M.; Hill, R. M. *Curr. Opin. Colloid Interface Sci.* **2006**, *11*, 193–202.
- Roach, P.; Shirtcliffe, N. J.; Newton, M. I. *Soft Matter* **2008**, *4*, 224–240.
- Xia, F.; Jiang, L. *Adv. Mater.* **2008**, *20*, 2842–2858.
- Wenzel, R. N. *Ind. Eng. Chem.* **1936**, *28*, 988–994.
- Cassie, A. B. D.; Baxter, S. *Trans. Faraday Soc.* **1944**, *40*, 546–551.
- Baxter, S.; Cassie, A. B. D. *J. Text. Ind.* **1945**, *36*, T67–90.
- Yan, H.; Kurogi, K.; Mayama, H.; Tsujii, K. *Angew. Chem., Int. Ed.* **2005**, *44*, 3453–3456.
- Kurogi, K.; Yan, H.; Mayama, H.; Tsujii, K. *J. Colloid Interface Sci.* **2007**, *312*, 156–163.
- Darmanin, T.; Taffin de Givenchy, E.; Amigoni, S.; Guittard, F. *Langmuir* **2010**, DOI: 10.1021/la103310m, in press.
- Darmanin, T.; Guittard, F. *Langmuir* **2009**, *25*, 5463–5466.
- (a) Darmanin, T.; Nicolas, M.; Guittard, F. *Langmuir* **2008**, *24*, 9739–9746. (b) Darmanin, T.; Nicolas, M.; Guittard, F. *Phys. Chem. Chem. Phys.* **2008**, *10*, 4322–4326.
- (a) Darmanin, T.; Guittard, F. *J. Am. Chem. Soc.* **2009**, *131*, 7928–7933. (b) Zenerino, A.; Darmanin, T.; Taffin de Givenchy, E.; Amigoni, S.; Guittard, F. *Langmuir* **2010**, *26*, 13545–13549. (c) Darmanin, T.; Guittard, F. *J. Mater. Chem.* **2009**, *19*, 7130–7136. (d) Darmanin, T.; Guittard, F. *J. Colloid Interface Sci.* **2009**, *335*, 146–149.
- Taffin de Givenchy, E.; Guittard, F.; Bracon, F.; Cambon, A. *Liq. Cryst.* **1999**, *26*, 1163–1170.
- (a) Fornasieri, G.; Guittard, F.; G ribaldi, S. *Liq. Cryst.* **2004**, *31*, 1–5. (b) Fornasieri, G.; Guittard, F.; G ribaldi, S. *Liq. Cryst.* **2003**, *30*, 251–257.
- Caillier, L.; Guittard, F.; Taffin de Givenchy, E.; G ribaldi, S. *Mol. Cryst. Liq. Cryst.* **2005**, *437*, 71–80.
- Ho-Hoang, A.; Schulz, E.; Fache, F.; Boiteux, G.; Lemaire, M. *J. Mater. Chem.* **1996**, *6*, 1107–1112.
- Ho-Hoang, A.; Fache, F.; Lemaire, M. *Synth. Commun.* **1996**, *2*, 1289–1304.
- Ho-Hoang, A.; Fache, F.; Boiteux, G.; Lemaire, M. *Synth. Met.* **1994**, *62*, 277–280.
- Hamley, I. W. *Introduction to Soft Matter. Polymer, Colloids, Amphiphiles and Liquid Crystals*; Wiley-VCH Verlag GmbH & Co. KGaA: Weinheim, 2000; Chapter 5.
- Guo, Z.-G.; Liu, W.-M. *Appl. Phys. Lett.* **2007**, *90*, 223111.
- Balu, B.; Breedveld, V.; Hess, D. W. *Langmuir* **2008**, *24*, 4785–4790.
- (a) Feng, L.; Zhang, Y.; Xi, J.; Zhu, Y.; Wang, N.; Xia, F.; Jiang, L. *Langmuir* **2008**, *24*, 4114–4119. (b) Cho, W. K.; Choi, I. S. *Adv. Funct. Mater.* **2008**, *18*, 1089–1096.